STRUCTURAL COMPROMISE IN SPIKING CORTEX AND CONNECTED NETWORKS

Ella Sahlas, HBSc[*1], Tamir Avigdor, MSc[*2,3], Alexander Ngo, BSc[1], Jessica Royer, PsyD[1], Sara Larivière, PhD[4], Judy Chen, BHSc[1], Ke Xie, MSc[1], Yezhou Wang, MSc[1], Jack Lam, MDCM, MSc[1], Raúl Rodríguez-Cruces, MD, PhD[1], Thaera Arafat, MD[1], Raluca Pana, MD[5], Andrea Bernasconi, MD[6], Neda Bernasconi, MD, PhD[6], Birgit Frauscher, MD, PhD[†3], Boris C. Bernhardt, PhD[†1]

[1]*Multimodal Imaging and Connectome Analysis Laboratory, McConnell Brain Imaging Centre, Montreal Neurological Institute and Hospital, McGill University, Montreal, QC, Canada*
[2]*Analytical Neurophysiology Laboratory, Montreal Neurological Institute and Hospital, McGill University, Montreal, QC, Canada*
[3]*Department of Neurology, Duke University School of Medicine, Durham, NC, USA*
[4]*Sherbrooke Laboratory for Integrative Connectomics, Centre de Recherche du CHUS, Université de Sherbrooke, Sherbrooke, QC, Canada*
[5]*Department of Neurology and Neurosurgery, Montreal Neurological Institute and Hospital, McGill University, Montreal, QC, Canada*
[6]*Neuroimaging of Epilepsy Laboratory, McConnell Brain Imaging Centre, Montreal Neurological Institute and Hospital, McGill University, Montreal, QC, Canada*
[*]*Joint first authors*; [†]*Joint senior authors*

RUNNING TITLE

Structural compromise in spiking cortex

Correspondence to:

Boris C. Bernhardt, PhD
Montreal Neurological Institute and Hospital (NW-254)
3801 University Street, Montreal, QC H3A 2B4, Canada
e: boris.bernhardt@mcgill.ca / p: (514) 398-3579

Ella Sahlas, MD-PhD student
e: ella.sahlas@mail.mcgill.ca

ABSTRACT

INTRODUCTION. Epilepsy is increasingly conceptualized as a network disorder, and advancing methods for its diagnosis and treatment requires characterizing both the epileptic generator and related networks. We combined multimodal magnetic resonance imaging (MRI) and high-density electroencephalography (HD-EEG) to interrogate alterations in cortical microstructure, morphology, and local function within and beyond spiking tissue in focal epilepsy. **METHODS.** We studied 25 patients with focal epilepsy (12F, mean ± SD age = 31.28 ± 9.30 years) and 55 age- and sex-matched healthy controls, subdivided into a group of 30 for imaging feature normalization (15F, 31.40 ± 8.74 years) and a group of 25 for replication (12F, 31.04 ± 5.65 years). The 3T MRI acquisition included T1-weighted, diffusion, quantitative T1 relaxometry, and resting-state functional imaging. Open-access MRI processing tools derived cortex-wide maps of morphology and microstructure (cortical thickness, mean diffusivity, and quantitative T1 relaxometry) and intrinsic local function and connectivity (timescales, connectivity distance, and node strength) for all participants. Multivariate approaches generated structural and functional alteration scores for each cortical location. Using HD-EEG, the predominant spike type was localized and we quantified MRI alterations within spike sources, as well as in proximal and connected networks. **RESULTS.** Regions harboring spike sources showed increased structural MRI alterations (mean: 27.98%) compared to the rest of the brain (mean: 17.67%) in patients. Structural compromise extended to all regions with close functional coupling to spike sources (paired *t*-tests; FDR-corrected $p < 0.05$), but not to anatomical neighbors of spike sources. This finding was replicated using average control functional, structural, and anatomical matrices instead of patient-specific matrices. **CONCLUSION.** Spiking regions contain more marked alterations in microstructure and morphology than the remaining cortex, which may help localize the epileptogenic zone non-invasively. There are nevertheless broader networks effects, which may relate to a cascading of structural changes to functionally connected cortices. These results underscore the utility of combining high-definition MRI and EEG approaches for characterizing epileptogenic tissue and assessing distributed network effects.

KEYWORDS: Structural imaging, Functional imaging, Connectome, Magnetic Resonance Imaging, Electroencephalography, Epileptic spikes, Focal epilepsy

INTRODUCTION

Epilepsy is increasingly conceptualized as both a structural and functional disorder, and advancing its diagnosis and treatment requires characterizing epileptic lesions as well as related networks[1,2]. This is mirrored in the methods used to study epilepsy, of which high-field MRI and HD-EEG are among the most advanced, providing unprecedented spatial and temporal precision[3,4]. Surprisingly, these two modalities have rarely been combined despite their potential synergy in identifying epileptic tissue. Translation of recent advances in non-invasive neuroimaging into clinically viable methods promises to facilitate epilepsy diagnosis, support surgical planning, and elucidate focal epilepsies deemed non-lesional using conventional tools[1,2,5,6,7]. Localizing lesions and networks that harbor epileptogenic activity is especially critical to deliver adequate care to patients with pharmaco-resistant seizures, which affect over 30% of people with epilepsy[8,9]. Poor seizure control reduces quality of life and increases the risk of premature death[8,10,11]. In pharmaco-resistant epilepsy, surgical resection of the region responsible for seizures—the epileptogenic zone—is the most effective treatment to control seizures and improve quality of life[12,13,14], yet it remains critically underutilized. Only about 1% of potential surgical candidates undergo epilepsy surgery each year in high-income countries[15,16], and even fewer are operated in middle- and low-income countries[17]. While drug-resistant epilepsy syndromes can often be successfully treated via targeted surgical resections, these conditions also involve large-scale brain networks, with potential implications for surgical prognosis[5].

A major factor explaining the underutilization of surgery to treat pharmaco-resistant focal epilepsy lies in the challenge of safely and precisely localizing the epileptogenic zone[2]. This is notably due to the paucity of quantitative markers for the epileptogenic zone that are non-invasive, accurate, and effective. Improved characterization of the epileptogenic zone would be useful clinically, especially in cases considered "imaging-negative". Neurophysiological work has indicated that localization of interictal epileptic spikes via HD-EEG can localize the epileptogenic zone[4]. Interictal spikes are more frequent, stable, and safe markers than recorded seizures, and HD-EEG offers more complete brain coverage than intracranial recordings, with fewer complication risks[18]. Meanwhile, functional MRI studies indicate widespread changes in both local and network function. Recent work in temporal lobe epilepsy suggests marked decreases in intrinsic neural timescales bilaterally[19]. Long-range connectivity, measured with connectivity distance metrics, has also been found to be reduced, mainly ipsilateral to the seizure focus[20]. Node strength, a measure of global network integration, has been shown to co-localize with epileptogenicity in certain patients[21]. Beyond these functional effects, there are increasingly detailed accounts of structural alterations in gray and white matter in focal epilepsy. These involve changes in cortical morphology and microstructure, notably bilateral cortical thickness changes extending beyond the affected lobe in temporal and extra-temporal epilepsy[22,23], together with changes in quantitative MRI proxies of cortical myelination in the former[24,25]. These findings are complemented by data showing perturbations in the integrity of cortico-subcortical diffusivity, indicating microstructural alterations, in several epilepsy syndromes[26,27,28].

Despite a rich literature describing electrical, hemodynamic, and structural alterations in epilepsy, there is a lack of studies systematically profiling the neurophysiological epileptic focus and connected regions. Current characterization of epileptic focus and associated networks, thus, remains subject to several limitations. First, many studies assessing alterations across the entire brain in epilepsy do not test whether alterations are most prominent in patient-specific, EEG-defined epileptic foci[19,20,22,24,26]. Additional research is needed to determine whether epileptic foci located via EEG are epicenters of alterations in microstructure, morphology, and intrinsic local function. Second, previous research has not systematically examined brain regions with functional, structural, and anatomical relationships to EEG-defined epileptic foci[4,21]. Consistent with the reframing of epilepsy as a network disorder, the magnitude of alterations across brain regions may relate to their degree of coupling to epileptic generators. Third, much of the existing literature does not capitalize on combinations of modalities to optimize both spatial and temporal resolution in mapping epileptogenicity. Prior MRI research has structurally profiled disease epicentres defined via imaging[28,29] rather than electrical activity. Here, we address these gaps by quantifying microstructural, morphological, and functional changes measured via high-field MRI within and beyond epileptic spike sources defined by HD-EEG. We further quantify epilepsy-related alterations in adjacent regions as well as functionally and structurally connected neighbors of spike sources to investigate network-level effects.

METHODS

Participants

We recruited 25 adult patients diagnosed with focal epilepsy who underwent both multimodal 3T MRI and HD-EEG at the Montreal Neurological Institute and Hospital. The patient cohort included 12 women and 13 men, with a mean age ± standard deviation (SD) of 31.28 ± 9.30 years. The diagnoses at discharge from the epilepsy monitoring unit indicated that the source of seizures was temporal in 14 cases, frontal in 5, fronto-temporal in 3, and temporo-occipital in 3. Thirteen cases were right-lateralized and 12 cases were left-lateralized. Thirteen patients later underwent epilepsy surgery. In all operated patients, there was lobe and laterality concordance between the spike source and the resection (8 patients) or thermocoagulation (5 patients). We also recruited 55 age- and sex-matched healthy adults as control participants, divided into two independent control cohorts. The control cohort whose data served for normalization of MRI features (n = 30) included 15 women and 15 men, with a mean age ± SD of 31.40 ± 8.74 years. The control cohort whose data served for replication of findings (n = 25) included 12 women and 13 men, with a mean age ± SD of 31.04 ± 5.65 years. Control participants underwent the same multimodal 3T MRI as patients and had no history of neurological or psychiatric conditions.

MRI data acquisition

MRI data were obtained in patients and control participants using a 3T Siemens Magnetom Prisma Fit scanner with a 64-channel head coil receiver. We acquired T1-weighted (T1w) scans via a three-dimensional magnetization-prepared rapid gradient-echo (3D-MPRAGE) sequence (repetition time (TR) = 23000 ms, echo time (TE) = 3.14 ms, inversion time (TI) = 900 ms, flip angle = 9º, matrix = 320 x 320, voxel size = 0.8 x 0.8 x 0.8 mm^3, field of view (FOV) = 256 x 256 mm^2, 224 sagittal slices). Diffusion-weighted imaging (DWI) data were obtained using a two-dimensional spin-echo-based echo-planar imaging sequence with multi-band acceleration, based on three shells with b-values of 300 (10 diffusion weighting directions), 700 (40 diffusion directions), and 2000 (90 diffusion directions) s/mm^2 (TR = 3500 ms, TE = 64.40 ms, flip angle = 90º, refocusing flip angle = 180º, voxel size = 1.6 x 1.6 x 1.6 mm^3, FOV = 224 x 224 mm^2, slice thickness = 1.6 mm, multi-band factor = 3, echo spacing = 0.76 ms). Quantitative T1 relaxometry was acquired via a 3D-MP2RAGE sequence (TR = 5000 ms, TE = 2.90 ms, T1 1 = 940 ms, T1 2 = 2830 ms, flip angle 1 = 4º, flip angle 2 = 5º, matrix = 320 x 320, voxel size = 0.8 x 0.8 x 0.8 mm^3, FOV = 256 x 256 mm^2, 240 sagittal slices, echo spacing = 7.2 ms, bandwidth = 270 Hx/pixel). Resting-state functional MRI (rsfMRI) was acquired using a two-dimensional blood-oxygen-level-dependent (2D-BOLD) echo-planar sequence with multi-band acceleration (TR = 600 ms, TE = 30 ms, flip angle = 52º, matrix = 80 x 80, voxel size = 3 x 3 x 3 mm^3, FOV = 240 x 240 mm^2, slice thickness = 3 mm, multi-band factor = 6, echo spacing = 0.54 ms, bandwidth = 2084 Hz/pixel, 48 slices oriented to the bicommissural line minus 30 degrees). For the ~7-minute duration of the rsfMRI scan, participants fixated a cross displayed in the centre of the screen and were instructed to not fall asleep.

MRI data processing

3T MRI data were processed using Micapipe (version 0.2.0, http://micapipe.readthedocs.io)[30] to extract surface-based measures of cortical microstructure, morphology, and local function (**Figure 1A**).

T1w scans were reoriented to standard orientation, deobliqued, corrected for intensity nonuniformity, intensity normalized, and skull stripped. We generated cortical surface models from native T1w scans for each patient using FreeSurfer (version 6.0, https://surfer.nmr.mgh.harvard.edu)[31]. Manual quality control was conducted to correct for segmentation errors in surface extraction via placement of control points and manual edits. Vertex-wise native maps of cortical thickness (CT) were generated in native surface space for each patient by computing the Euclidian distance separating corresponding pial and white matter vertices.

Using MRtrix, DWI images were denoised, b0 intensity-normalized, and corrected for susceptibility distortion, head motion, and eddy currents[32]. Native maps of diffusion tensor-derived mean diffusivity (MD) were generated via interpolation of MD along the surface.

For qT1 relaxometry, 14 equivolumetric surfaces were generated between the pial matter and the white matter boundaries, and qT1 image intensities were sampled systematically using these surfaces. We, thus, obtained vertex-wise profiles of quantitative T1 relaxation time (qT1).

Using Connectome Workbench[33], we registered native cortical features (CT, MD, and qT1) to the fsLR-5k template surface, with 5000 vertices per hemisphere. We applied spatial smoothing (Gaussian kernel, full width at half maximum (FWHM) = 10 mm) to the resulting CT, MD, and qT1 surface maps.

We processed rsfMRI via AFNI (https://afni.nimh.nih.gov) and FSL (https://fsl.fmrib.ox.ac.uk/fsl), including image reorientation, correction for motion and distortion, removal of nuisance variable signal, averaging of volumetric timeseries, boundary-based registration to native FreeSurfer space, and mapping to surface space using trilinear interpolation[34,35]. Spatial smoothing was also applied (Gaussian kernel, FWHM = 10 mm). To ensure magnetic field saturation, we discarded the first five volumes in each rsfMRI scan.

For each patient, we derived a vertex-wise functional connectivity (FC) matrix by cross-correlating rsfMRI time series, a vertex-wise structural connectivity (SC) matrix from DWI using MRtrix, and a vertex-wise geodesic distance (GD) matrix from T1w imaging using Dijkstra's algorithm, as previously described[30]. We applied Fischer's r-to-z transformation to the correlation coefficients in the FC matrix.

Vertex-wise maps of intrinsic neural timescale (INT) were computed for each patient from rsfMRI timeseries using an autocorrelation function[19]. Maps of connectivity distance coefficient (CDC) were generated by thresholding the FC to retain the top 10% of connections, then correlating GD coefficients with the thresholded FC coefficients[20]. Node strength (NS) maps were computed by summing the weights of all connections for each vertex in the FC[21].

HD-EEG data acquisition and processing

HD-EEG recordings were acquired overnight during the patient's hospitalization for pre-surgical evaluation in the epilepsy monitoring unit. Recordings were acquired using a Nihon Koden system (Tokyo, Japan) with 83 electrodes glued with collodion, placed according to the 10–10 EEG system, and sampled at 1000 Hz[36]. Impendences were kept below 1 kΩ for the selected electrodes. The signal was filtered using a Butterworth band-pass filter between 0.3 Hz and 70 Hz. Electrode positions were digitized on the scalp of the patients using a Polhemus localizer device (Vermont, USA). Then, the electrodes were aligned on the head model using reference points (nasion, right, and left ear). Co-registration was refined via a surface fitting approach using Brainstorm[37]. The lead field matrix was computed using the boundary element method with 3 layers for brain, skull, and scalp (with conductivities of 0.33, 0.0165, and 0.33 S/m)[36], using OpenMEEG implemented in Brainstorm.

Spike source localization

An experienced epileptologist (B. F.) marked spikes at their peak. The average predominant spike type was localized at the time of maximum amplitude using coherent maximum entropy on the mean (MEM)[38]. MEM is a nonlinear distributed technique for solving the EEG inverse problem. The reference model for coherent MEM is built using a data-driven clustering of the cortical surface into K parcels[4]. We used previously derived FreeSurfer segmentations. To estimate coefficients quantifying the contribution of each dipolar source to the data, we employed the multivariate source pre-localization method[39]. This allowed modelling of the probability of each parcel being active. The ability of coherent MEM to capture the spatial extent of underlying generators has been thoroughly assessed in prior work[4]. Nearest-neighbor interpolation propagated signal probability maps to the same fsLR-5k template surface as the multiparametric MRI data. In each patient, the spike source was defined as vertices with a signal amplitude > 50% of the mean amplitude at the time of maximum spike amplitude, resulting in a binarized map (**Figure 1B**).

Mapping MRI alteration scores

In each patient, we computed vertex-wise Mahalanobis distances comparing the multivariate aggregate of CT, MD, and qT1 values against corresponding values in 30 control participants. We thus obtained a vertex-wise structural alteration score (**Figure 2A**). Likewise, we computed a functional alteration score based on the Mahalanobis distance aggregating INT, CDC, and NS in patients relative to controls (**Figure 2B**).

Mapping spike sources and their functional, structural, and anatomical neighbors

From the FC, SC, and GD matrices of each patient, we extracted the functional coupling, structural connectivity, and geodesic distance profiles of the spike source relative to all vertices in the rest of the cortex. For each patient, we identified all vertices with above-median functional coupling, structural connectivity, and geodesic proximity to the spike source. We grouped these vertices into ten groups with weights within the 5th to 50th percentile of functional coupling, structural connectivity, and geodesic proximity to the spike source (**Figure 2D**). For assessment of replication, we repeated this procedure using the averaged FC, SC, and GD matrices of the independent cohort of 25 control participants.

Quantifying MRI alterations in HD-EEG spike sources and their neighbors

We compared the percentage of vertices with significantly altered structural and functional Mahalanobis scores within the spike source to that of the rest of the cortex. The percentage of structurally altered vertices within spike sources was computed as the percent of outlier Mahalanobis distances for CT, MD, and qT1 among all vertices within the spike source. Outlier Mahalanobis distances were defined at the 5% level. Similarly, the percentage of structurally altered vertices in the rest of the cortex was calculated as the percent of outlier CD, MD, and qT1 Mahalanobis distances among all vertices outside of the spike source. The percentages of functionally altered vertices within spike sources and in the rest of the brain was computed as in the structural analysis, using percents of outlier Mahalanobis distances for INT, CDC, and NS. Additionally, we compared structural alteration multivariate scores within regions highly functionally coupled, structurally connected, or geodesically close to the spike source to scores across the rest of the cortex, using patient-specific FC, SC, and GD matrices. We replicated these comparisons using the normative matrices. Comparisons were performed using paired-samples *t*-tests. False Discovery Rate (FDR) corrections were applied to control for multiple comparisons.

Standard protocol approvals, registrations, and patient consents

Research ethics board approval. The Research Ethics Board of the Montreal Neurological Institute and Hospital approved this research involving human participants.

Informed consent. All participants in the study provided written informed consent.

Data availability

Preprocessed cortical thickness, diffusion, and quantitative relaxometry maps used in the study will be made available on the Open Science Framework upon publication.

RESULTS

Structural MRI alteration analysis within and beyond HD-EEG spike sources

Cortex within patient-specific spike sources was compared to cortex beyond these sources across all 25 patients (**Figure 3A**). This comparison revealed a greater percentage of structurally altered vertices within epileptic spike sources than across the rest of cortex (mean: 27.98% versus mean: 17.67%; paired *t*-test; $t = 2.28$; $p = 0.036$).

We assessed whether electroclinical focus location was related to structural alterations within spike sources. Thirteen patients had a greater percentage of structural alterations within the spike source. These patients presented with heterogeneous lobar distribution of electroclinical foci, with foci in temporal (7), frontal (4), and fronto-temporal (2) regions. In 7 of these patients, foci were left-lateralized, and in 6, foci were right-lateralized. The 12 patients who did not have a greater percentage of structural alterations within the spike source had electronical foci in temporal (7), frontal (1), fronto-temporal (1), temporo-occipital (2), and

occipital (1) regions; half were left-lateralized and half were right-lateralized. Concordance between structural alterations and HD-EEG spike sources was thus independent of lateralization (χ^2 test; $\chi^2 = 0.00$; $p = 1.00$) and lobar distribution of the electroclinical focus (χ^2 test; $\chi^2 = 5.10$; $p = 0.277$).

Functional MRI alteration analysis within and beyond HD-EEG spike sources

There was a subtle increase in the percentage of functionally altered vertices in spike sources compared to the rest of the cortex, but the percentages did not differ significantly (mean: 10:37% versus mean: 7.67%; paired *t*-test; $t = 1.15$; $p = 0.263$; **Figure 3B**).

Structural alteration analysis in functional, structural, and anatomical neighbors of spike sources

To determine whether the structural compromise identified within spike sources may extend to connected regions, we compared cortex within functional, structural, and anatomical neighbors of spike sources to the rest of the cortex. We located all vertices beyond the spike source that had above-median functional, structural, or anatomical proximity to the spike source. For each of the three neighbor types, we then partitioned all of these vertices into ten groups with decreasing proximity to the spike source. We quantified alterations within each of these ten graded groups of vertices for every neighbor type.

Among the ten groups of vertices with above-median functional coupling to the spike source, all showed higher percentages of structurally altered vertices than the rest of the cortex, paired *t*-tests, $p_{FDR} < 0.05$. The mean percentages of structurally altered vertices in regions with highest to lowest functional coupling to the spike source are depicted in **Figure 4A** (*left*).

Of the ten groups of vertices with above-median structural connectivity to the spike source, eight showed higher percentages of structurally altered vertices than the rest of the cortex, paired *t*-tests, $p_{FDR} < 0.05$. **Figure 4A** (*middle*) details the mean percentages of structurally altered vertices in regions with the most to the fewest structural connections to the spike source.

Of the ten groups of vertices with above-median anatomical proximity to the spike source, none showed higher percentages of structurally altered vertices than the rest of the cortex, paired *t*-tests, $p_{FDR} > 0.05$, as illustrated in **Figure 4A** (*right*).

Replication analysis substituting patient-specific connectivity for normative connectivity matrices

Lastly, we assessed whether structural alteration findings in neighbors in spike sources could be replicated using average healthy control functional coupling, structural connectivity, and anatomical distance matrices instead of patient-specific matrices. Normative matrices were generated from the independent cohort of healthy control participants.

Using normative functional connectivity, all ten groups of vertices with above-median functional coupling to the spike source showed higher percentages of structurally altered vertices than the rest of the cortex, paired *t*-tests, $p_{FDR} < 0.05$, as shown in **Figure 4B** (*left*).

With normative structural connectivity, only one of the ten groups of vertices with above-median structural connectivity to the spike source contained a higher percentage of structurally altered vertices than the rest of the cortex, paired *t*-tests, $p_{FDR} < 0.05$. The mean percentages of structurally altered vertices in these regions are represented in **Figure 4B** (*middle*).

Among the ten groups of vertices with above-median normative anatomical proximity to the spike source, none showed higher percentages of structurally altered vertices than the rest of the cortex, paired *t*-tests, $p_{FDR} > 0.05$, as shown in **Figure 4B** (*right*).

In sum, structural alteration findings were replicated in functional and anatomical neighbors, but not structural connectivity neighbors, across two methods of computing functional coupling, structural connectivity, and anatomical distance matrices: the patient-specific approach and an approach averaging matrices across healthy control participants. Both methods were consistent with the presence of structural alterations in functional neighbors of spike sources, and the lack thereof in anatomical neighbors.

DISCUSSION

Capitalizing on multiple imaging features and on both spatial and temporal detail, our findings chart a map of focal epilepsies characterized by *(i)* increased structural—but not functional—compromise captured by MRI within EEG-defined spike sources, and *(ii)* extension of structural compromise to regions functionally coupled to—but not solely anatomically nearby—spike sources. Taken together, these findings incite additional multimodal studies analyzing both epileptogenic tissue and related networks. Results also highlight the potential for synergy between MRI and HD-EEG for identifying epileptogenic tissue, which may help advance non-invasive and seizure-independent epilepsy diagnostics. Prior investigations have improved the accuracy of non-invasive approaches in localizing epileptogenicity by combining modalities[40,41,42]. Nonetheless, epilepsy research has more commonly remained siloed across neurophysiology and imaging domains. Consequently, while neurophysiology research has developed increasingly reliable methods for localizing epileptogenic activity, whether through iEEG[43] or HD-EEG[4], MRI research has focused on mapping lesions, which do not always coincide with the epileptogenic zone[42]. There is a marked paucity of studies investigating MRI measures in EEG-defined epileptogenic regions, yet approaches of this kind are requisite for deciphering the structural makeup of cortex harboring seizures. This is illustrated in the use of both structural imaging and stereotactic EEG data in the generation of personalized virtual brain models[2]. Morphological alterations have also been found to modulate circuit excitability in computational models of epilepsy[44], which may drive circuits to generate epileptic activity. Multimodal approaches combining MRI and HD-EEG also carry potential for clinical impact. HD-EEG offers multiple opportunities for non-invasively localizing the epileptogenic zone[4,41], while high-field MRI is unparalleled in detecting subtle, epilepsy-causing lesions[45,46,47]. Together, these modalities hold potential to locate the surgical target in cases where conventional methods may not contribute to diagnosis and surgical target definition. This combination could also ultimately help limit or more precisely target invasive pre-surgical investigations in an increasing number of patients with pharmaco-resistant epilepsy.

The present study suggests that regions harboring EEG spike sources contain MRI-derived microstructural and morphological alterations. This is in line with studies that have applied machine learning methods to localizing epileptogenic lesions based on data extracted from MRI[45,46,47]. Much of this literature has focused on automating the detection of focal cortical dysplasia, which often still eludes conventional MRI evaluations[45]. To validate localization approaches, prior studies have trained models such as feed-forward artificial neural networks on morphometric maps[45] and deep convolutional neural networks on T1w and fluid-attenuated inversion recovery images[46]. MRI-based localization approaches have become increasingly successful yet have generally remained limited in several ways. First, studies rarely validate MRI approaches against electroclinical evidence. Instead, studies commonly use lesions segmented from MRI as the ground truth. This introduces potential confounds as methods are developed and tested using the same MRI data. Rarely, studies validate approaches based on histopathological data[47], but additional validation based on spike sources defined electrically *in vivo* is scarcely reported. The approach presented in our study could provide context for the integration of neurophysiological benchmarks into future studies validating MRI-based detection algorithms. Second, accuracy rates of automated lesion localization average approximately 80% at most[45,46,47]. Careful feature selection and weighting may introduce clinically meaningful improvements in accuracy rates. The present study is motivated by prior literature highlighting epilepsy-related changes in cortical thickness, relaxometry, and diffusion parameters[22,24,26]. Our findings are consistent with increased alterations in these features within the epileptic focus, providing grounds for their inclusion in future lesion detection work. Our study does not find evidence of significantly increased alterations in MRI-sensitive intrinsic function within spike sources. Additional studies in larger samples may be required to detect possible changes in MRI-derived metrics of intrinsic function localized to spike sources. Consistent with existing evidence, alterations in intrinsic function may be widely distributed across the cortex[19,20] and less concentrated within spike sources relative to structural changes, thus, differences across spiking and non-spiking tissue may be more subtle and difficult to detect.

Prior research has characterized network-related disruptions in epilepsy[19,20,22,24,26,48]. Alterations in intrinsic neural timescales, cortical thickness, and diffusion properties have been shown to extend bilaterally in patients with temporal lobe epilepsy and other epilepsy syndromes[19,22,26]. Recent work in temporal lobe

epilepsy has identified widespread age-related changes in cortical thickness and diffusion metrics, extending beyond the ipsilateral mesiotemporal lobe[48]. Prior investigations have also identified alterations in connectivity distance and relaxometry extending to ipsilateral regions beyond the seizure focus[20,24]. Still, little work has tested whether alteration epicenters correspond to connectivity neighbors of the epileptic focus. Certain studies have assessed epilepsy-related disruptions in structural networks[49] and evaluated the impact of connectivity profiles on atrophy patterns[50]. However, no study to date has quantified structural alteration patterns with functional and anatomical relationships to the electrically defined spike source. Our study addresses this gap via a novel method for multiparametric alteration scoring, in cortex with varying connections to the spike source. Our findings are consistent with the absence of increased alterations in the geodesic neighbors of spike sources, indicating that the patterning of the microstructural signature of epileptic activity may not be explained simply by proximity to spike sources. In our study, alterations were more frequently identified in functional than in structural neighbors of spike sources, suggesting that regions of microstructural damage may be linked by polysynaptic more than monosynaptic connections. Longitudinal structure-function studies are needed to ascertain whether this reflects pre-existing structural irregularities in functional networks or alterations induced by the propagation of chronic seizures. Previously described disease-specific changes in structural networks[49] may explain the contrasting presence of alterations in most patient-specific structural connectivity neighbors and lack thereof in most normative structural connectivity neighbors. Our study identified increased microstructural alterations in regions with above-median functional coupling to regions harboring spike sources, suggesting a possible cascading of microstructural alterations to cortical regions beyond spike sources through functional network effects. This finding is consistent with focal epilepsy invading large-scale networks, while also highlighting a possible limitation of using structural imaging in isolation to localize epilepsy-related alterations: MRI alone may identify false positives, particularly when only a single modality is used. However, used in combination with electrophysiological data and clinical correlates, quantitative multimodal MRI carries potential to identify otherwise undetectable lesions and help guide surgical planning[7,29,47].

The present study highlights MRI-derived alterations in cortical microstructure and morphology that co-localize with epileptic spike sources, and that cascade into polysynaptic functional networks in which spike sources are embedded. Intrinsic functional alterations, on the other hand, may be distributed more broadly, with less specific co-localization than structural changes. While results are overall consistent with synergy of HD-EEG and high-field MRI findings in identifying epilepsy-related alterations, additional work is recommended to optimize the weighting of modalities and imaging parameters across epilepsy syndromes and individual patients. These findings will advance current conceptions of focal epilepsy and help to uncover clinically relevant network effects that may impact treatment and prognosis.

ACKNOWLEDGMENTS

E.S. acknowledges funding from the Fonds de Recherche du Québec – Santé (FRQS) Doctoral Training Scholarship. B.F. was supported by a salary award (Chercheur-boursier clinicien Senior) from FRQS and a project grant from the Canadian Institutes of Health Research (CIHR) (PJT-175056). B.C.B. acknowledges funding from CIHR (FDN-154298, PJT-174995), the Natural Sciences and Engineering Research Council of Canada (NSERC) (Discovery-1304413), FRQS, the Brain Canada Foundation, the SickKids Foundation (NI17-039), the Azrieli Center for Autism Research (ACAR), the Helmholtz International BigBrain Analytics and Learning Laboratory (HIBALL), and the Canada Research Chairs Program.

AUTHOR CONTRIBUTIONS

E.S. and B.C.B. contributed to the conception and design of the study; E.S., T.A., A.N., J.R., S.L., J.C., B.F., and B.C.B. contributed to data acquisition; E.S. and T.A. contributed to the processing of MRI and EEG data, respectively; E.S. and B.C.B. contributed to data analysis and manuscript writing; all authors revised and approved the manuscript.

POTENTIAL CONFLICTS OF INTEREST

None to disclose

REFERENCES

1. Royer J, Bernhardt BC, Larivière S, et al. Epilepsy and brain network hubs. *Epilepsia*. 2022;63(3):537-550. doi:10.1111/epi.17171

2. Jirsa V, Wang H, Triebkorn P, et al. Personalised virtual brain models in epilepsy. *Lancet Neurol*. 2023;22(5):443-454. doi:10.1016/S1474-4422(23)00008-X

3. Bernasconi A, Bernasconi N. The role of MRI in the treatment of drug-resistant focal epilepsy. *Eur Neurol*. 2022;85(5):333-341. doi:10.1159/000525262

4. Avigdor T, Abdallah C, von Ellenrieder N, et al. Fast oscillations >40 Hz localize the epileptogenic zone: An electrical source imaging study using high-density electroencephalography. *Clin Neurophysiol*. 2021;132(2):568-580. doi:10.1016/j.clinph.2020.11.031

5. Larivière S, Park BY, Royer J, et al. Connectome reorganization associated with temporal lobe pathology and its surgical resection. *Brain*. 2024;147(7):2483-2495. doi:10.1093/brain/awae141

6. Larivière S, Bernasconi A, Bernasconi N, Bernhardt BC. Connectome biomarkers of drug-resistant epilepsy. *Epilepsia*. 2021;62(1):6-24. doi:10.1111/epi.16753

7. Jin P, Wu D, Li X, Ren L, Wang Y. Towards precision medicine in epilepsy surgery. *Ann Transl Med*. 2016;4(2):24. doi:10.3978/j.issn.2305-5839.2015.12.65

8. Löscher W, Potschka H, Sisodiya SM, Vezzani A. Drug resistance in epilepsy: Clinical impact, potential mechanisms, and new innovative treatment options. *Pharmacol Rev*. 2020;72(3):606-638. doi:10.1124/pr.120.019539

9. Feigin VL, Nichols E, Alam T, et al. Global, regional, and national burden of neurological disorders, 1990-2016: A systematic analysis for the Global Burden of Disease Study 2016. *Lancet Neurol*. 2019;18(5):459-480. doi:10.1016/S1474-4422(18)30499-X

10. Fazel S, Wolf A, Långström N, Newton CR, Lichtenstein P. Premature mortality in epilepsy and the role of psychiatric comorbidity: A total population study. *Lancet*. 2013;382(9905):1646-1654. doi:10.1016/S0140-6736(13)60899-5

11. Hamilton KJ, Chen Z, Tomlin A, Kwan P. Mortality and morbidity of patients with treated and untreated epilepsy in New Zealand. *Epilepsia*. 2020;61(3):519-527. doi:10.1111/epi.16435

12. Thijs RD, Surges R, O'Brien TJ, Sander JW. Epilepsy in adults. *Lancet*. 2019;393(10172):689-701. doi:10.1016/S0140-6736(18)32596-0

13. Sheng J, Liu S, Qin H, Li B, Zhang X. Drug-resistant epilepsy and surgery. *Curr Neuropharmacol*. 2018;16(1):17-28. doi:10.2174/1570159X15666170504123316

14. Rugg-Gunn F, Miserocchi A, McEvoy A. Epilepsy surgery. *Pract Neurol*. 2020;20(1):4-14. doi:10.1136/practneurol-2019-002192

15. Samanta D, Ostendorf AP, Willis E, et al. Underutilization of epilepsy surgery: Part I: A scoping review of barriers. *Epilepsy Behav*. 2021;117:107837. doi:10.1016/j.yebeh.2021.107837

16. Engel J Jr. The current place of epilepsy surgery. *Curr Opin Neurol*. 2018;31(2):192-197. doi:10.1097/WCO.0000000000000528

17. Watila MM, Xiao F, Keezer MR, et al. Epilepsy surgery in low- and middle-income countries: A scoping review. *Epilepsy Behav*. 2019;92:311-326. doi:10.1016/j.yebeh.2019.01.001

18. Arya R, Mangano FT, Horn PS, Holland KD, Rose DF, Glauser TA. Adverse events related to extraoperative invasive EEG monitoring with subdural grid electrodes: A systematic review and meta-analysis. *Epilepsia*. 2013;54(5):828-839. doi:10.1111/epi.12073

19. Xie K, Royer J, Larivière S, et al. Atypical intrinsic neural timescales in temporal lobe epilepsy. *Epilepsia*. 2023;64(4):998-1011. doi:10.1111/epi.17541

20. Larivière S, Weng Y, Vos de Wael R, et al. Functional connectome contractions in temporal lobe epilepsy: Microstructural underpinnings and predictors of surgical outcome. *Epilepsia*. 2020;61(6):1221-1233. doi:10.1111/epi.16540

21. Courtens S, Colombet B, Trébuchon A, Brovelli A, Bartolomei F, Bénar CG. Graph measures of node strength for characterizing preictal synchrony in partial epilepsy. *Brain Connect*. 2016;6(7):530-539. doi:10.1089/brain.2015.0397

22. Galovic M, de Tisi J, McEvoy AW, et al. Resective surgery prevents progressive cortical thinning in temporal lobe epilepsy. *Brain*. 2020;143(11):3262-3272. doi:10.1093/brain/awaa284

23. Hong SJ, Bernhardt BC, Schrader DS, Bernasconi N, Bernasconi A. Whole-brain MRI phenotyping in dysplasia-related frontal lobe epilepsy. *Neurology*. 2016;86(7):643-650. doi:10.1212/WNL.0000000000002374

24. Bernhardt BC, Fadaie F, Vos de Wael R, et al. Preferential susceptibility of limbic cortices to microstructural damage in temporal lobe epilepsy: A quantitative T1 mapping study. *Neuroimage*. 2018;182:294-303. doi:10.1016/j.neuroimage.2017.06.002

25. Royer J, Larivière S, Rodríguez-Cruces R, et al. Cortical microstructural gradients capture memory network reorganization in temporal lobe epilepsy. *Brain*. 2023;146(9):3923-3937. doi:10.1093/brain/awad125

26. Hatton SN, Huynh KH, Bonilha L, et al. White matter abnormalities across different epilepsy syndromes in adults: An ENIGMA-Epilepsy study. *Brain*. 2020;143(8):2454-2473. doi:10.1093/brain/awaa200

27. Liu M, Bernhardt BC, Hong SJ, Caldairou B, Bernasconi A, Bernasconi N. The superficial white matter in temporal lobe epilepsy: A key link between structural and functional network disruptions. *Brain*. 2016;139(Pt 9):2431-2440. doi:10.1093/brain/aww167

28. Hong SJ, Bernhardt BC, Caldairou B, et al. Multimodal MRI profiling of focal cortical dysplasia type II. *Neurology*. 2017;88(8):734-742. doi:10.1212/WNL.0000000000003632

29. Larivière S, Schaper FLWVJ, Royer J, et al. Brain networks for cortical atrophy and responsive neurostimulation in temporal lobe epilepsy. *JAMA Neurol*. Published online September 30, 2024. doi:10.1001/jamaneurol.2024.2952

30. Rodríguez-Cruces R, Royer J, Herholz P, et al. Micapipe: A pipeline for multimodal neuroimaging and connectome analysis. *Neuroimage*. 2022;263:119612. doi:10.1016/j.neuroimage.2022.119612

31. Dale AM, Fischl B, Sereno MI. Cortical surface-based analysis. I. Segmentation and surface reconstruction. *Neuroimage*. 1999;9(2):179-194. doi:10.1006/nimg.1998.0395

32. Tournier JD, Smith R, Raffelt D, et al. MRtrix3: A fast, flexible and open software framework for medical image processing and visualisation. *Neuroimage*. 2019;202:116137. doi:10.1016/j.neuroimage.2019.116137

33. Glasser MF, Sotiropoulos SN, Wilson JA, et al. The minimal preprocessing pipelines for the Human Connectome Project. *Neuroimage*. 2013;80:105-124. doi:10.1016/j.neuroimage.2013.04.127

34. Cox RW. AFNI: Software for analysis and visualization of functional magnetic resonance neuroimages. *Comput Biomed Res*. 1996;29(3):162-173. doi:10.1006/cbmr.1996.0014

35. Jenkinson M, Beckmann CF, Behrens TE, Woolrich MW, Smith SM. FSL. *Neuroimage*. 2012;62(2):782-790. doi:10.1016/j.neuroimage.2011.09.015

36. Avigdor T, Abdallah C, Afnan J, et al. Consistency of electrical source imaging in presurgical evaluation of epilepsy across different vigilance states. *Ann Clin Transl Neurol*. 2024;11(2):389-403. doi:10.1002/acn3.51959

37. Tadel F, Baillet S, Mosher JC, Pantazis D, Leahy RM. Brainstorm: A user-friendly application for MEG/EEG analysis. *Comput Intell Neurosci*. 2011;2011:879716. doi:10.1155/2011/879716

38. Amblard C, Lapalme E, Lina JM. Biomagnetic source detection by maximum entropy and graphical models. *IEEE Trans Biomed Eng*. 2004;51(3):427-442. doi:10.1109/TBME.2003.820999

39. Mattout J, Pélégrini-Issac M, Garnero L, Benali H. Multivariate source prelocalization (MSP): Use of functionally informed basis functions for better conditioning the MEG inverse problem. *Neuroimage*. 2005;26(2):356-373. doi:10.1016/j.neuroimage.2005.01.026

40. Rossi Sebastiano D, Tassi L, Duran D, et al. Identifying the epileptogenic zone by four non-invasive imaging techniques versus stereo-EEG in MRI-negative pre-surgery epilepsy patients. *Clin Neurophysiol*. 2020;131(8):1815-1823. doi:10.1016/j.clinph.2020.05.015

41. Li Y, Fogarty A, Razavi B, et al. Impact of high-density EEG in presurgical evaluation for refractory epilepsy patients. *Clin Neurol Neurosurg*. 2022;219:107336. doi:10.1016/j.clineuro.2022.107336

42. Zijlmans M, Zweiphenning W, van Klink N. Changing concepts in presurgical assessment for epilepsy surgery. *Nat Rev Neurol*. 2019;15(10):594-606. doi:10.1038/s41582-019-0224-y

43. Jaber K, Avigdor T, Mansilla D, et al. A spatial perturbation framework to validate implantation of the epileptogenic zone. *Nat Commun*. 2024;15(1):5253. doi:10.1038/s41467-024-49470-z

44. Tejada J, Garcia-Cairasco N, Roque AC. Combined role of seizure-induced dendritic morphology alterations and spine loss in newborn granule cells with mossy fiber sprouting on the hyperexcitability of a computer model of the dentate gyrus. *PLoS Comput Biol*. 2014;10(5):e1003601. doi:10.1371/journal.pcbi.1003601

45. David B, Kröll-Seger J, Schuch F, et al. External validation of automated focal cortical dysplasia detection using morphometric analysis. *Epilepsia*. 2021;62(4):1005-1021. doi:10.1111/epi.16853

46. Gill RS, Lee HM, Caldairou B, et al. Multicenter validation of a deep learning detection algorithm for focal cortical dysplasia. *Neurology*. 2021;97(16):e1571-e1582. doi:10.1212/WNL.0000000000012698

47. Hong SJ, Kim H, Schrader D, Bernasconi N, Bernhardt BC, Bernasconi A. Automated detection of cortical dysplasia type II in MRI-negative epilepsy. *Neurology*. 2014;83(1):48-55. doi:10.1212/WNL.0000000000000543

48. Chen J, Ngo A, Rodríguez-Cruces R, et al. A worldwide ENIGMA study on epilepsy-related gray and white matter compromise across the adult lifespan. Preprint. *bioRxiv*. 2024;2024.03.02.583073. doi:10.1101/2024.03.02.583073

49. Larivière S, Royer J, Rodríguez-Cruces R, et al. Structural network alterations in focal and generalized epilepsy assessed in a worldwide ENIGMA study follow axes of epilepsy risk gene expression. *Nat Commun*. 2022;13(1):4320. doi:10.1038/s41467-022-31730-5

50. Larivière S, Rodríguez-Cruces R, Royer J, et al. Network-based atrophy modeling in the common epilepsies: A worldwide ENIGMA study. *Sci Adv*. 2020;6(47):eabc6457. doi:10.1126/sciadv.abc6457

TABLE

	Patient cohort	**Normalization control cohort**	**Replication control cohort**
Number	25	30	25
Sex (F/M)	12/13	15/15	12/13
Age at scan (years)	31.28 ± 9.30	31.40 ± 8.74	31.04 ± 5.65
Lateralization (L/R)	13/12	N/A	N/A

Table 1. Participant demographics.

FIGURE LEGENDS

Figure 1. Overview of procedures for multimodal feature extraction. (**a**) Synopsis of multiparametric 3T MRI data acquisition, processing, and features of interest. Acquisition of 3D-MPRAGE, DWI, 3D-MP2RAGE, and 2D-BOLD sequences. Processing using open access software tools: Micapipe (version 0.2.0) and FreeSurfer (version 6.0). Extraction of quantitative features: cortical thickness, mean diffusivity, T1 relaxation time; rsfMRI metrics of intrinsic neural timescale, connectivity distance coefficient, and node strength. Surface-based sampling of cortical thickness between the pial and white matter surfaces; mean diffusivity, quantitative T1 relaxation time, and rsfMRI metrics at the mid-thickness surface. Surfaces are overlaid on the volumetric images of the same patient as in Figure 2. (**b**) Synopsis of HD-EEG data acquisition and processing. Overnight HD-EEG recording using an 83-electrode system. Signal processing using cMEM, then thresholding and binarization to extract vertices with signal amplitude > 50% of the mean at time of maximum spike amplitude for localization of spike sources.

Figure 2. Multivariate scoring of structural and functional alterations and identification of functional, structural, and anatomical neighbors of spike sources. (**a**) Patient-specific map of the multivariate score for alterations in cortical microstructure and morphology, computed as the Mahalanobis distance of cortical thickness (CT), mean diffusivity (MD), and quantitative T1 relaxation time (qT1) at each vertex in the patient relative to the control cohort. For illustration: univariate map of vertex-wise alterations in CT, computed as the z-score of CT at each vertex relative to the control cohort; univariate map of vertex-wise alterations in MD and univariate map of vertex-wise alterations in qT1, computed similarly. Each map is shown in the same representative patient. (**b**) Patient-specific map of the multivariate score for alterations in local functional properties of the cortex, computed as the Mahalanobis distance of intrinsic neural timescale (INT), connectivity distance coefficient (CDC), and node strength (NS) at each vertex relative to the control cohort. For illustration: univariate map of vertex-wise alterations in INT, computed as the z-score of INT at each vertex relative to the control cohort; univariate map of vertex-wise alterations in CDC and univariate map of vertex-wise alterations in NS, computed similarly. Each map is shown in the same representative patient. (**c**) Spike source localized using HD-EEG via coherent maximum entropy on the mean in the same patient. (**d**) Vertices with the 5th to 50th percentiles of functional coupling weights to the spike source (*left*), vertices with the 5th to 50th percentiles of structural connectivity strength to the spike source (*middle*), and vertices with the 5th to 50th percentiles of anatomical proximity to the spike source (*right*).

Figure 3. Structural and functional profiling of cortex within spike sources. (**a**) Comparison of the percentage of structurally altered vertices within patient-specific spike sources and in cortex beyond these sources. (**b**) Comparison of the percentage of functionally altered vertices within patient-specific spike sources and in cortex beyond these sources.

Figure 4. Structural alterations in neighbors of spike sources. (**a**) Quantification of the percentage of structurally altered vertices within functional coupling neighbors (*left*), structural connectivity neighbors (*middle*), and anatomical neighbors (*right*) of spike sources, and comparison to cortex beyond spike sources. Among the ten groups of vertices with above-median functional coupling to the spike source, all showed significantly higher percentages of structurally altered vertices than the rest of the cortex, paired *t*-tests; *t* ranged from 2.35-3.75; FDR-corrected *p* ranged from 0.006-0.028. The mean percentages of structurally altered vertices ranged from 19.13-21.27%. Of the ten groups of vertices with above-median structural connectivity to the spike source, eight showed significantly higher percentages of structurally altered vertices than the rest of the cortex and two were trending, paired *t*-tests; $t = 1.97$-4.36; FDR-corrected $p = 0.002$-0.060. The mean percentages of structurally altered vertices were 18.65-22.03%. Among the ten groups of vertices with above-median anatomical proximity to the spike source, none showed significantly higher percentages of structurally altered vertices than the rest of the cortex, paired *t*-tests; FDR-corrected $p > 0.05$. (**b**) Replication via healthy control (normative) functional coupling, structural connectivity, and geodesic distance: quantification of the percentage of structurally altered vertices within normative functional coupling neighbors (*left*), normative structural connectivity neighbors (*middle*), and normative anatomical neighbors (*right*) of spike sources, and comparison to cortex beyond spike sources. Using normative functional connectivity, all ten groups of vertices with above-median functional coupling to the spike source showed significantly higher percentages of structurally altered vertices than the rest of the cortex, paired *t*-tests; $t = 2.25$-3.82; FDR-corrected $p = 0.008$-0.034. The mean percentages of structurally altered vertices were 19.07-23.39%. With normative structural connectivity, one of the ten groups of vertices with above-median structural connectivity to the spike source contained a significantly higher percentage of structurally altered vertices than the rest of the cortex, paired *t*-tests; $t = 0.83$-3.29; FDR-corrected $p = 0.031$-0.413. The mean percentages of structurally altered vertices were 18.80-21.42%. Of the ten groups of vertices with above-median normative anatomical proximity to the spike source, none showed significantly higher percentages of structurally altered vertices than the rest of the cortex, paired *t*-tests; FDR-corrected $p > 0.05$.

Figure 1.

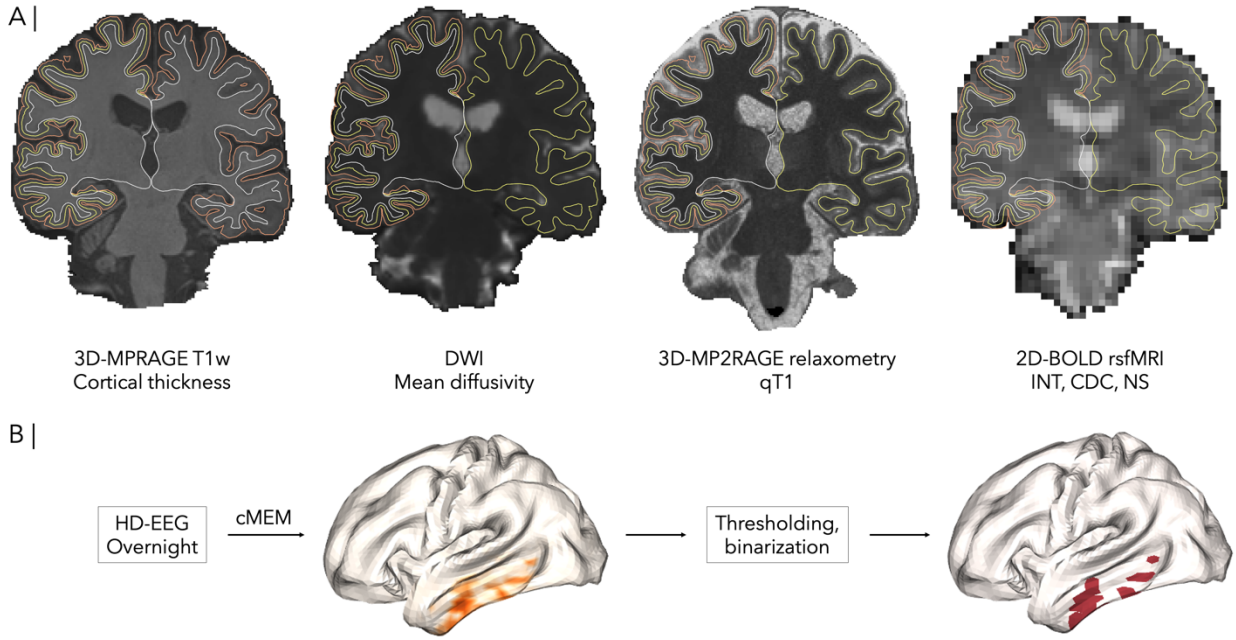
A |
3D-MPRAGE T1w
Cortical thickness
DWI
Mean diffusivity
3D-MP2RAGE relaxometry
qT1
2D-BOLD rsfMRI
INT, CDC, NS
B |
HD-EEG
Overnight
cMEM
Thresholding,
binarization

Figure 2.

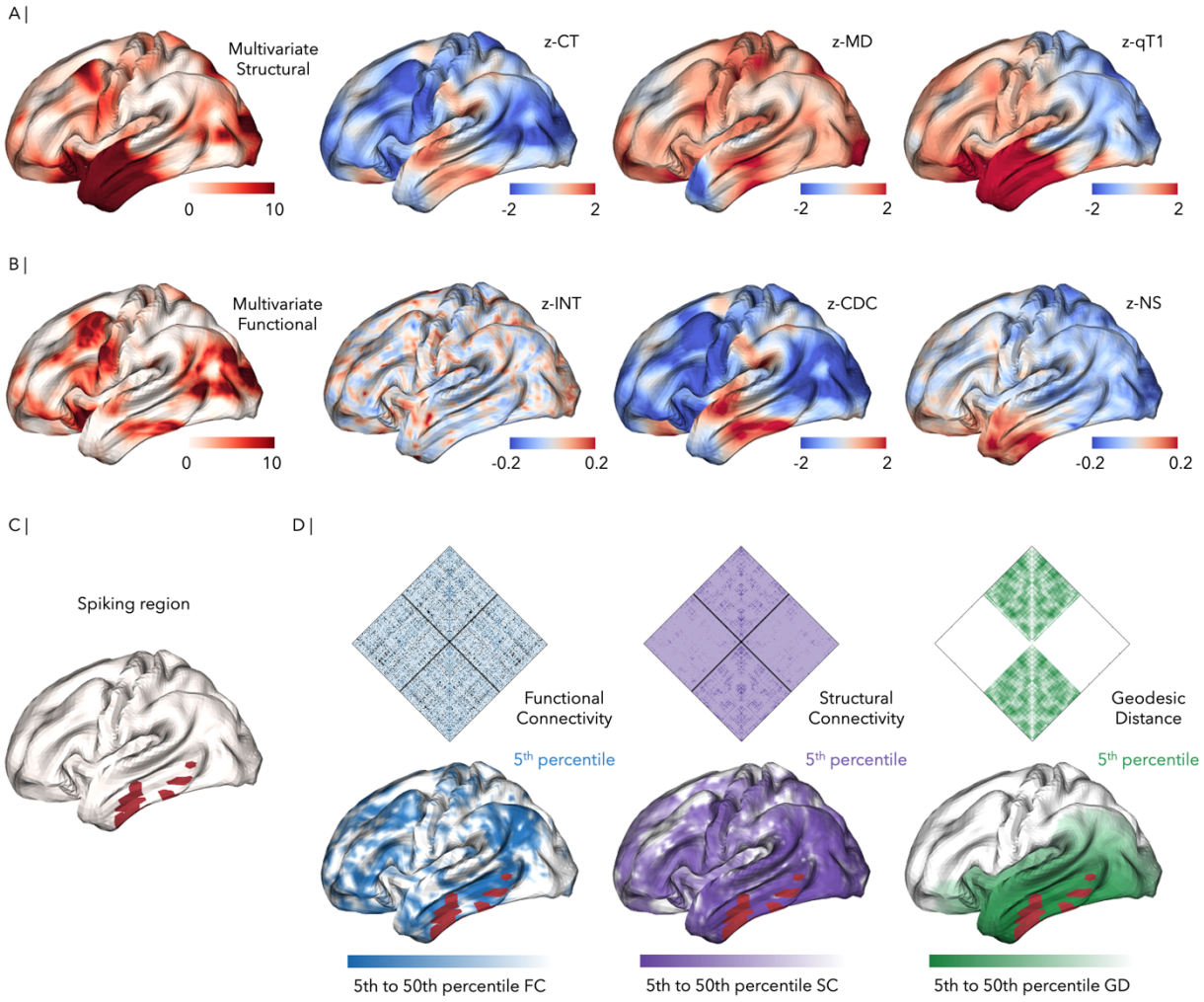
A |
Multivariate Structural
0
10
z-CT
-2
2
z-MD
-2
2
z-qT1
-2
2
B |
Multivariate Functional
0
10
z-INT
-0.2
0.2
z-CDC
-2
2
z-NS
-0.2
0.2
C |
Spiking region
D |
Functional Connectivity
Structural Connectivity
Geodesic Distance
5th percentile
5th percentile
5th percentile
5th to 50th percentile FC
5th to 50th percentile SC
5th to 50th percentile GD

Figure 3.

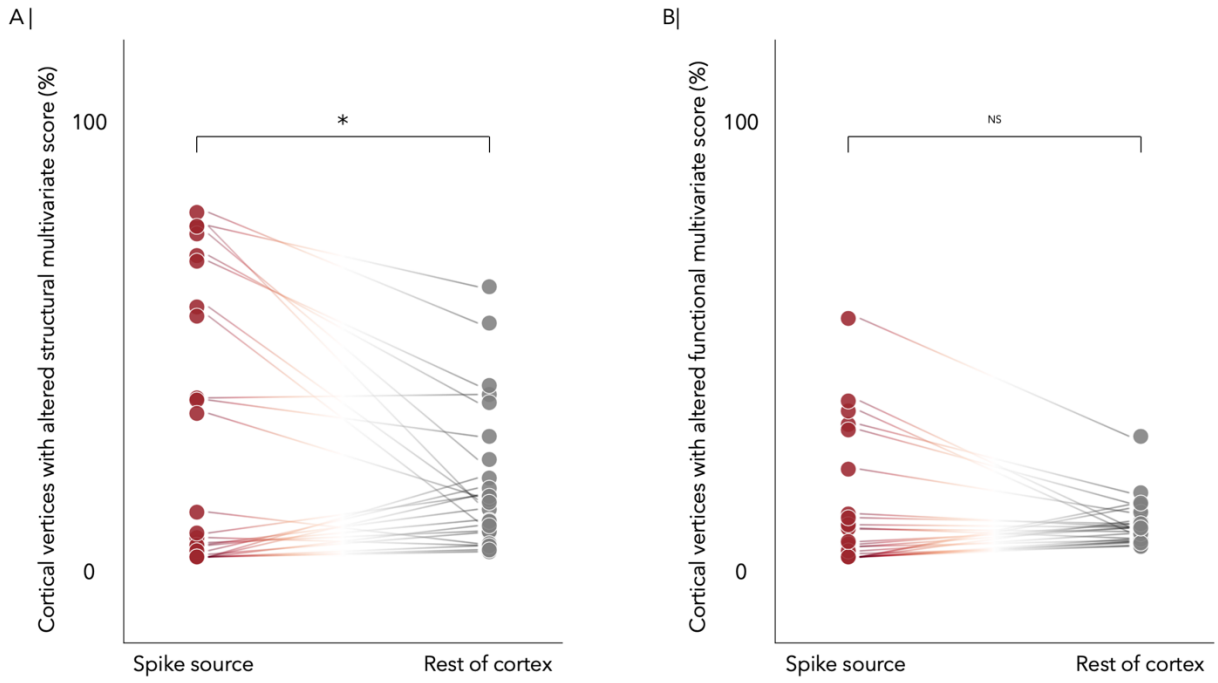
A |
Cortical vertices with altered structural multivariate score (%)
100
0
*
Spike source
Rest of cortex
B|
Cortical vertices with altered functional multivariate score (%)
100
0
NS
Spike source
Rest of cortex

Figure 4.

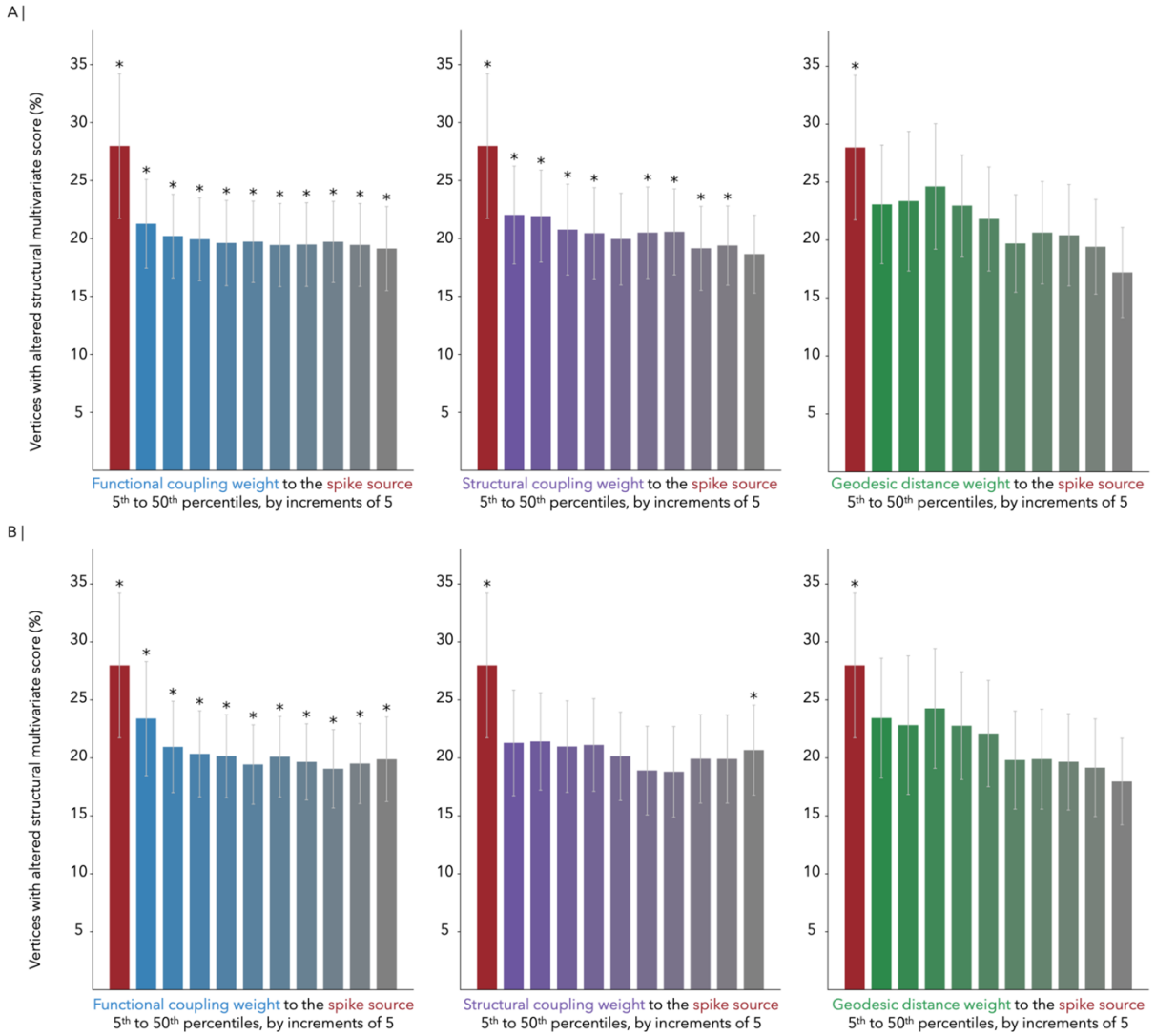
A |
B |
Vertices with altered structural multivariate score (%)
35
30
25
20
15
10
5
Functional coupling weight to the spike source
5th to 50th percentiles, by increments of 5
Structural coupling weight to the spike source
5th to 50th percentiles, by increments of 5
Geodesic distance weight to the spike source
5th to 50th percentiles, by increments of 5